ELSEVIER

Electrical Power and Energy Systems 27 (2005) 465–471

ELECTRICAL POWER & ENERGY SYSTEMS

www.elsevier.com/locate/ijepes

A robust damping controller for SMES using loop-shaping technique

A.H.M.A. Rahim[a,*], E.P. Nowicki[b]

[a]Department of Electrical Engineering, K.F. University of Petroleum and Minerals, KFUPM Box 349, Dhahran 31261, Saudi Arabia
[b]Department of Electrical Engineering, University of Calgary, Calgary, Alta., Canada

Received 18 August 2002; revised 25 November 2004; accepted 2 February 2005

Abstract

A robust damping controller for a power system installed with super-conducting magnetic energy storage (SMES) has been designed using a simple graphical loop-shaping technique. The graphical method starts by selection of a nominal plant function satisfying the robust stability and performance criterion. The variations in operating conditions from the nominal values are modeled as multiplicative structured uncertainty. The generator-SMES system has been represented with a detailed dynamic model for the control design. The robust design, with generator speed variation as the controller input, was tested for a range of operating points considering various disturbances. It is observed that the fixed parameter robust controller provides very good damping for a wide range of operating conditions.

Keywords: SMES; Robust damping control; Loop-shaping method; Power system stabilization

1. Introduction

The application of super-conducting magnetic energy storage systems (SMES) to enhance power system stability was first proposed by Peterson [1]. The concept of operation of SMES is simple: a super-conducting coil is made to store or release energy by charging or discharging a thyristor-controlled power converter connected to an ac power system. The thyristor firing angles are varied in an appropriate manner for the energy exchange.

Successful commissioning of a 10 MW-30 MJ SMES unit by Bonneville Power Administration in its Pacific AC Intertie initiated widespread interest for SMES research in power system control applications [2,3]. A number of research articles demonstrated the ability of SMES to enhance system transient performance [4–9]. Control designs reported vary from classical linear control [6–8], nonlinear strategies and optimum control applications [4,9] and adaptive fuzzy and neural network applications [10,11]. PI controls exhibit damping improvements, but constant gains do not perform as good for varying system conditions [6]. The disadvantage of the linear controls for the nonlinear power system dynamics is the dependency of the control strategies on the points of linearization, necessitating 'robust' controllers for operation over a broader range. Robust controller design for large power systems, generally, is complicated because of the high order dynamics as well the mathematical complexity of the robustness considerations. This in turn requires sacrificing accuracy by considering lower order models. A relatively recent study of multi-area power systems through reduced order modeling has indicated that each area should be provided with an SMES unit [12]. In such event, each area of a power network can be represented in adequate detail and decentralized effective robust controller designs can be implemented.

This article presents a simple and a relatively new graphical technique of designing a robust SMES controller for damping power system transients. The design starts with a detailed dynamic model of the generator-SMES system. The variations in the operating conditions in the robust design have been modeled as multiplicative structured uncertainty. A graphical loop-shaping technique [13] combined with H_∞ techniques are employed to satisfy robust stability and performance criteria. The performance of the robust controller has been evaluated for various

* Corresponding author. Tel.: +966 3860 4986; fax: +966 3860 3535.
E-mail addresses: ahrahim@kfupm.edu.sa (A.H.M.A. Rahim), nowicki@enel.ucalgary.ca (E.P. Nowicki).

0142-0615/$ - see front matter © 2005 Elsevier Ltd. All rights reserved.
doi:10.1016/j.ijepes.2005.02.005

loading and disturbance conditions. The response exhibits extremely good damping properties with the proposed robust design.

2. The power system model

A synchronous generator connected to a large power system through a long transmission line, as shown in Fig. 1, is considered in this study. The generator is equipped with a static excitation system and is driven by a steam turbine. A super-conducting magnetic energy storage unit is connected to the generator bus.

The super-conducting magnetic storage system is a first generation flexible AC transmission system (FACTS) device. Electronically controlled FACTS devices have been widely researched and presently being implemented in power system applications for very fast and reliable control of voltages and power flows [14,15]. The SMES unit, configuration of which is given in Fig. 2a, contains a $\Delta-\Delta/\Delta-Y$ transformer, a 12-pulse converter bridge, and a super-conducting inductor. The converter can use GTO's instead of normal thyristors for wide range of firing angle control. Through the control of firing angles α_1 and α_2 of the cascaded converters, the dc voltages E_{d1} and E_{d2} and hence the real and reactive power outputs of the SMES can be varied simultaneously. Simulation tests showed that the reactive power injected by the SMES also plays an important role for system stabilization [16,17]. Simultaneous modulation of both real and reactive power gives not only damping of power swings but also damping of voltage oscillations in the network.

For the sake of simplicity of analysis, let us assume that the converters are operating at equal firing angle mode i.e. $\alpha_1=\alpha_2=\alpha$. The firing angle α, or the SMES voltage V_{SM}, is controlled through an additional controller as shown in Fig. 2b. The design of this controller, which should be 'robust' in terms of damping control for specific choices of the input signal, is given in the following sections. The block diagrams of the IEEE type 1 excitation system and the turbine-governor systems used for this study are given in Figs. 3 and 4, respectively. The four blocks in the governor-turbine system represent the speed relay, the servomotor, the steam chest, and the re-heater, respectively. The dynamic model of the synchronous generator is expressed in terms of four state variables involving the electromechanical swing

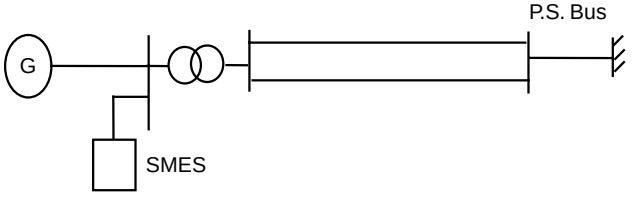

Fig. 1. Single machine infinite bus system.

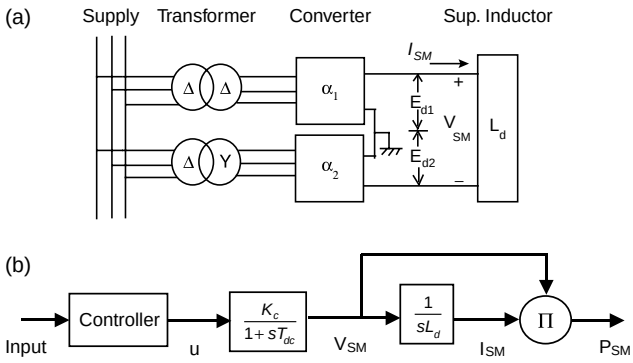

Fig. 2. (a) SMES unit schematic diagram, (b) Block diagram of the SMES control circuit.

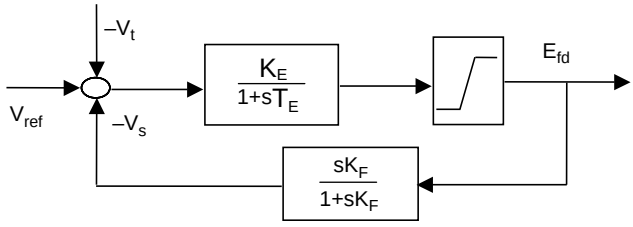

Fig. 3. IEEE type 1 excitation system.

equation and the internal voltage equations of the machine along the direct and quadrature axes.

The generator, the SMES, the excitation system, and the turbine-governor system equations can be combined to arrive at the composite dynamic model of a single machine infinite bus system as,

$$\dot{x} = f[x, u] \tag{1}$$

where, x is the vector of state variables $[\omega\ \delta\ e'_d\ e'_q\ E_{fd}\ V_s\ P_r\ P_s\ P_c\ P_m\ I_{SM}\ W_{SM}\ V_{SM}]^T$. The first four of the states correspond to those for the generator, followed by two for the excitation system, four for the governor-turbine system and the last three are for the SMES system. The system of Eq. (1) can be linearized around a nominal operating point to give,

$$\dot{x} = Ax + Bu \quad y = Cx \tag{2}$$

where, x and y are the perturbed states and the outputs of the system, respectively. The nominal plant transfer function between the input and selected output is expressed as,

$$P(s) = C[sI - A]^{-1}B \tag{3}$$

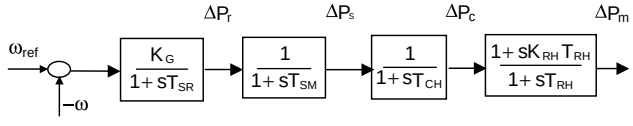

Fig. 4. Governor-turbine system block diagram.

3. Robust control design

The robust controller design for the SMES starts with a choice of a nominal operating point and calculation of the nominal plant function P given by Eq. (3). The variations in the operating conditions result in changes in A, B and C matrices and hence that in the plant function P. These perturbations are modeled as multiplicative uncertainties in this work. The robust design is then carried out using the minimization principles, H_∞ norms, and a graphical construction procedure called 'loop-shaping'. A brief theory of the uncertainty model, the robust stability criterion, and the graphical design technique are presented in this section. Finally, an algorithm for the control design is presented.

3.1. A. Uncertainty modeling

Suppose that the linearized plant having a nominal transfer function P belongs to a bounded set of transfer functions **P**. Consider that the perturbed transfer function resulting from the variations in operating conditions can be expressed in the form

$$\tilde{P} = (1 + \Omega W_2)P \tag{4}$$

Here, W_2 is a fixed stable transfer function, also called the weight, and Ω is a variable transfer function satisfying $\|\Omega\|_\infty < 1$. The infinity norm (∞-norm) of a function is the least upper bound of its absolute value, also written as $||\Omega||_\infty = \sup_\omega |\Omega(j\omega)|$, and is the largest value of gain on a Bode magnitude plot.

In the multiplicative uncertainty model (4), ΩW_2 is the normalized plant perturbation away from unity. If $\|\Omega\|_\infty < 1$, then,

$$\left|\frac{P(\tilde{j}\omega)}{P(jw)} - 1\right| \le |W_2(j\omega)|, \quad \forall\, \omega \tag{5}$$

So, $|W_2(j\omega)|$ provides the uncertainty profile, and in the frequency plane is the upper boundary of all the normalized plant transfer functions away from unity.

3.2. B. Robust stability and performance

Consider a multi-input control system given in Fig. 5. A controller C_R provides robust stability if it provides internal stability for every plant in the uncertainty set **P**. If L denotes

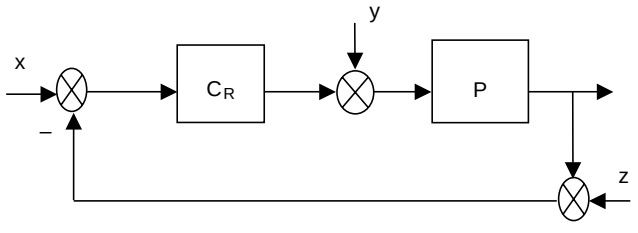

Fig. 5. Unity feedback plant with controller.

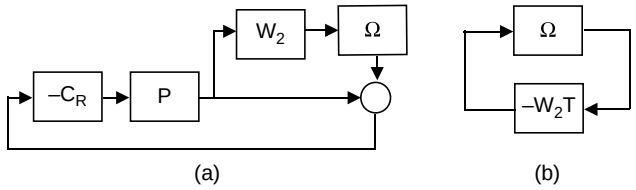

Fig. 6. Perturbed feedback system with controller and the reduced block diagram.

the open-loop transfer function ($L = PC_R$), then the sensitivity function S is written as,

$$S = \frac{1}{1 + L} \tag{6}$$

For a multiplicative perturbation model, robust stability condition is met if and only if $\|W_2T\|_\infty < 1$ [13,18]. This implies that,

$$\left|\frac{W_2(j\omega)L(j\omega)}{1 + L(j\omega)}\right| < 1, \quad \text{for all } \omega \tag{7}$$

T is the complement of S, and is the input–output transfer function.

The block diagram of a typical perturbed system, ignoring all inputs, is shown in Fig. 6a. The transfer function from output of Ω to the input of Ω is $-W_2T$. The properties of the block diagram can be reduced to those of the configuration given in Fig. 6b [19]. The maximum loop gain, $\|-W_2T\|_\infty$ is less than 1 for all allowable Ω, if and only if the small gain condition $\|W_2T\|_\infty < 1$ holds. The nominal performance condition for an internally stable system is given as $\|W_1S\|_\infty < 1$, where W_1 is a real-rational, stable, minimum phase transfer function, also called a weighting function. The robust performance condition is,

$$||W_2T||_\infty < 1, \quad \left\| \frac{W_1S}{1 + \Omega W_2T} \right\| < 1, \quad \forall\, ||\Omega|| < 1. \tag{8}$$

Combining all the above, it can be shown that a necessary and a sufficient condition for robust performance is [13],

$$|||W_1S| + |W_2T|||_\infty < 1 \tag{9}$$

3.3. C. The loop-shaping technique

Loop-shaping is a graphical procedure to design a proper controller C_R satisfying the robust stability and performance criteria given above. The basic idea of the method is to construct the loop transfer function L to satisfy the robust performance criterion approximately, and then to obtain the controller from the relationship $C_R = L/P$. Internal stability of the plants and properness of C_R constitute the constraints of the method. Condition on L is such that PC_R should not have any pole zero cancellation.

A necessary condition for robustness is that either or both $|W_1|$, $|W_2|$ must be less than 1 [18]. If we select a monotonically decreasing W_1 satisfying the other constraints on it, it can be shown that at low frequency

the open-loop transfer function L should satisfy,

$$|L| > \frac{|W_1|}{1-|W_2|} \tag{10}$$

while, for high frequency,

$$|L| < \frac{1-|W_1|}{|W_2|} \approx \frac{1}{|W_2|} \tag{11}$$

At high frequency $|L|$ should roll-off at least as quickly as $|P|$ does. This ensures properness of C_R. The general features of the open loop transfer function is that the gain at low frequency should be large enough for the steady state error, and $|L|$ should not drop-off too quickly near the crossover frequency resulting in internal instability.

3.4. D. The algorithm

The algorithm to generate a robust control function C_R involves the following steps.

1. From the linearized system find the nominal plant transfer function P.
2. Obtain the db-magnitude plot for the nominal as well as perturbed plant transfer functions.
3. Construct W_2 satisfying constraint (5).
4. Select W_1 as a monotonically decreasing, real, rational and stable function.
5. Choose L such that it satisfies conditions (10) and (11). The transition at crossover frequency should not be at slope steeper than -20 db/decade. Nominal internal stability is achieved if, on a Nyquist plot of L, the angle of L at crossover is greater than 180°.
6. Check for the nominal and robust performance criteria (8) and (9).
7. Construct the controller function from the relation $C_R = L/P$
8. Test for internal stability by direct simulation of the closed loop transfer function for pre-selected disturbance or input.
9. Repeat steps 5 through 8 until satisfactory L and C_R are obtained.

4. Evaluation of the robust controller

For robust control design, the speed variation of the generator ($\Delta\omega$) is considered as the input to the controller. In the collapsed plant-controller configuration of Fig. 5, P is constructed such that $\Delta\omega$ is its output. This $\Delta\omega$ signal constitutes the input to the controller C_R. For nominal generator power output of 0.8 pu at 0.85 lagging power factor the plant transfer function is obtained as,

$$P = \frac{-9.66s^3(s+z_1)(s+z_2)\ldots(s+z_8)}{s^2(s+p_1)(s+p_2)\ldots(s+p_{11})} \tag{12}$$

The non-zero zeroes and poles of the system, respectively are $[-217.3742, -42.208, -19.9073, -10.0484, -4.9857, -2.2638, -1.3278, -0.125]$, $[-218.72, -40.21 \pm j7.78, -18.9, -0.39 \pm j9.76, -10.29, -4.91, -1.53 \pm j0.68, -0.12]$. Two poles in the origin are contributed by the SMES, one by the integral relationship between SMES voltage and current, and the other through power and energy. Strictly speaking there is only one zero at the origin, the other two being the approximation of a real symmetric pair extremely close to the origin.

Off-nominal power output between the range of 0.2–1.2 pu and power factor of up to 0.8 lag/lead which gave steady state stable situations were considered in the robust design. The log-magnitude vs. frequency plots for the nominal and perturbed plants are shown in Fig. 7. Data for the generator-SMES system has been taken from [6].

The quantity $|\tilde{P}(j\omega)/P_{nom}(j\omega) - 1|$ is constructed for each perturbed plant $\tilde{P}(j\omega)$ and the upper envelope in the frequency plane is fitted to the function,

$$W_2(s) = \frac{89.1}{s^2 + 1.26s + 81} \tag{13}$$

A Butterworth filter, which satisfies the properties of $W_1(s)$, is selected as,

$$W_1(s) = \frac{K_c f_c^2}{s^3 + 2s^2 f_c + 2s f_c^2 + f_c^3} \tag{14}$$

Values of $K_c = 0.1$ and $f_c = 0.05$ were observed to be satisfy the requirement on the open loop transfer function L. For W_1 and W_2 selected above, and for a choice of the open-loop function L as,

$$L(s) = \frac{425s(s+42.205)(s+19.903)(s+217.3452)(s+4.9857)(s+10.0458)}{(s+18.9)(s+10.29)(s+4.91)(s+218.72)(s^2+80.42s+1677.3725)(s^2+3.06s+2.8033)} \tag{15}$$

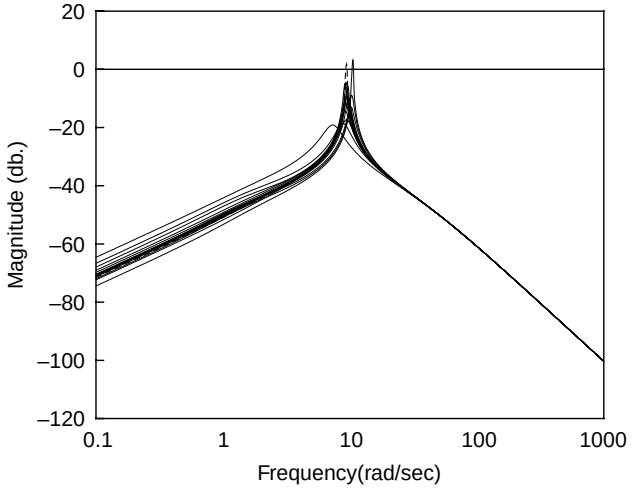

Fig. 7. Log-magnitude plots of nominal and perturbed plant transfer functions.

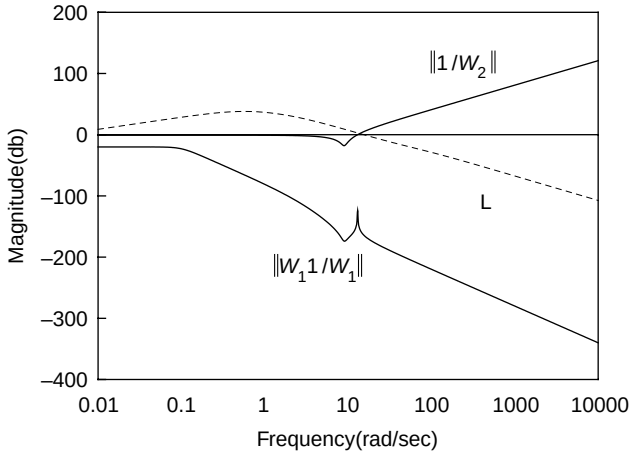

Fig. 8. Log-magnitude plots for the loop gain functions.

the controller transfer function obtained through the relation $C_R = L/P$ is,

$$C_R(s) = \frac{43.9958(s^2 + 0.78s + 95.4094)(s + 0.12)}{(s + 1.3278)(s + 2.2638)(s + 0.125)} \quad (16)$$

The log-magnitude plot relating W_1, W_2 for the upper and lower bounds of L given in (10) and (11) are shown in Fig. 8. The robust and nominal performance measures (8) and (9) for the robust designs are shown in Fig. 9. It can be observed that the nominal performance measure is very small relative to 0 db. The robust stability measure is marginally violated at the corner frequency. This is for a worst-case design in the absence of damping term in the electromechanical swing equation.

While selecting the open-loop transfer function, the internal stability of the plant in addition to the design criterion (8)–(11) had to be checked. A disturbance of 100% input torque pulse for 0.1 s on the generator shaft was simulated for this purpose. The rotor angle variations of the generator for the nominal operating point with and without the robust controller are plotted in Fig. 10. As can be

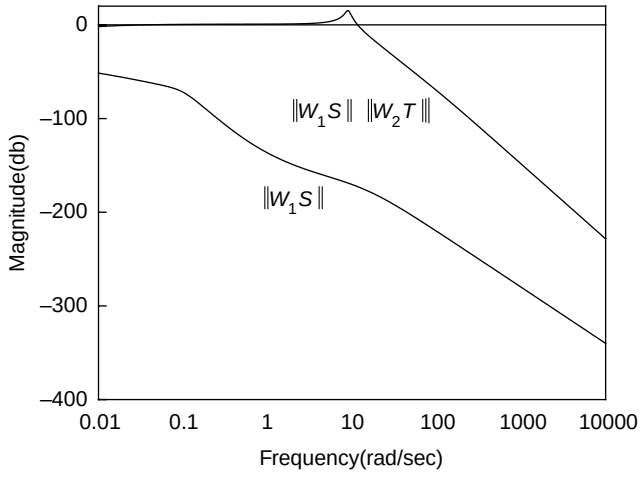

Fig. 9. The robust and nominal performance measures.

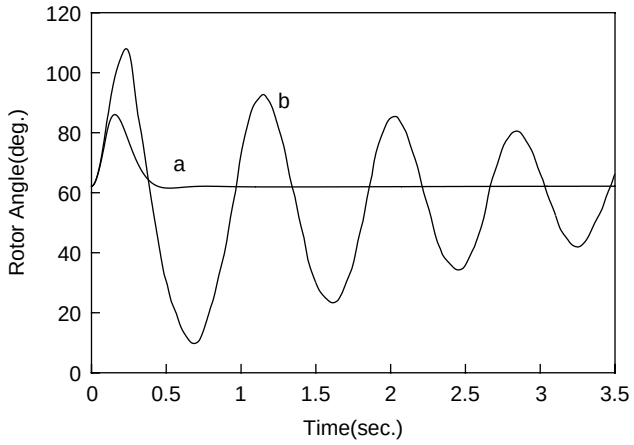

Fig. 10. Generator rotor angle variations for the nominal plant with, (a) proposed robust damping control, and (b) no control. The disturbance is a 100% torque pulse for 0.1 s.

observed, the robust controller provides extremely good damping to the rotor oscillations.

The robust controller designed was tested for a number of disturbances over a range of operating conditions. For a $3-\phi$ fault of 0.1 s on the remote bus, the rotor angle variations of the generator are plotted in Fig. 11. The pre-fault loading of the generator is 1.2 pu at 0.85 lagging power factor. Without the control the system is first swing unstable, while the robust controller is able to stabilize the system in a very short period. The operation mode of the SMES can be understood from examination of the variation of its energy storage as depicted in Fig. 12. The excess energy in the system charges up the SMES at the initiation of the fault, followed by subsequent discharge phase.

The robust controller was tested for its damping characteristics for a number of loading conditions and for different disturbances. Figs. 13 and 14 show the rotor angle and terminal voltage variations of the synchronous generator, respectively for a 100% input torque pulse for 0.1 s

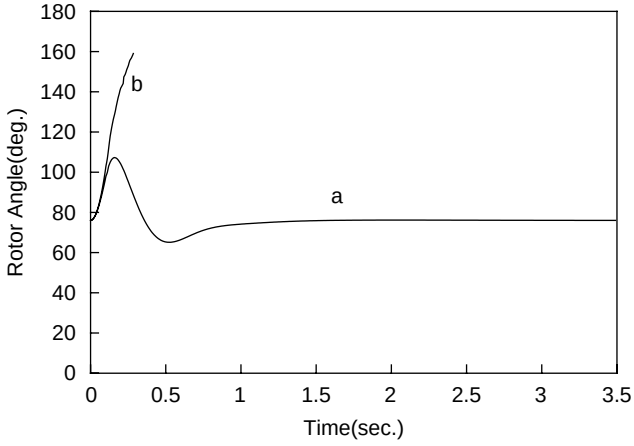

Fig. 11. Generator rotor angle variations following a three-phase fault on the remote bus for 0.1 s with, (a) proposed robust damping controller, and (b) no control.

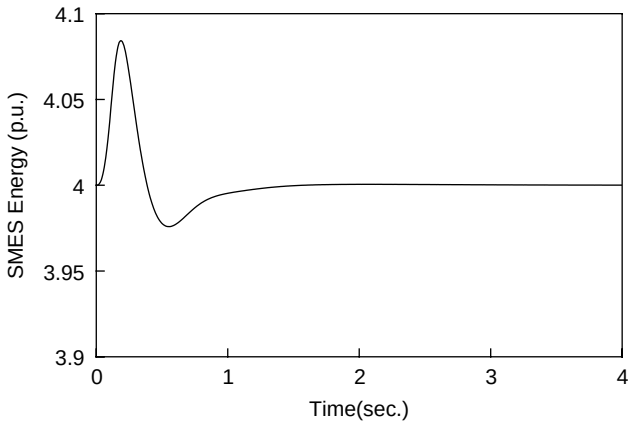

Fig. 12. SMES energy variation corresponding to the three-phase fault condition of Fig. 11.

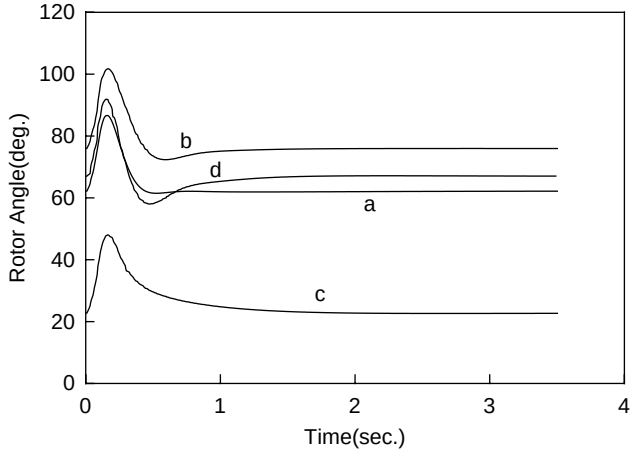

Fig. 13. Comparison of generator rotor angle characteristics with the proposed damping controller for a 100% input torques step for 0.1 s with, (a) at nominal operating condition of 0.8 pu output, (b) at 1.2 pu power, (c) at 0.2 pu power, and (d) for a three-phase fault on remote bus for 0.1 s at rated load.

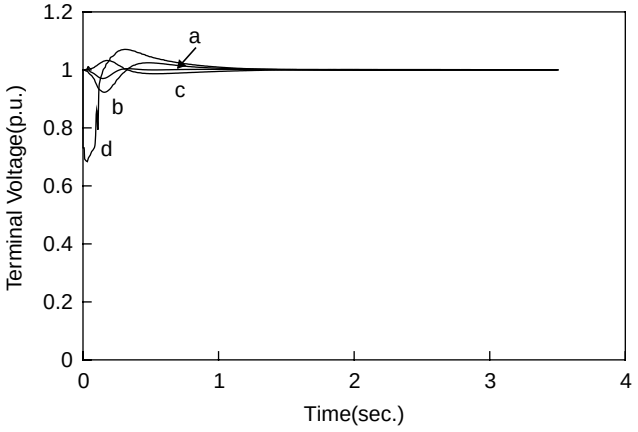

Fig. 14. Terminal voltage variations of the generator corresponding to Fig. 13.

and also for three-phase fault conditions. Comparative results for a 100% input torque pulse for 0.1 s for the following loading are presented; (a) nominal operating condition of 0.8 pu power at 0.85 power factor lag, (b) 1.2 pu power at 0.85 lagging pf, (c) 0.2 pu power at unity pf. The transient response following a three-phase fault for 0.1 s duration at rated load and 0.8 lagging pf are given by (d). It can be observed that good damping properties can be obtained with the robust speed feedback controller over a wide range of operating conditions. While the controller could be designed to provide even more damping, it would have to be compromised with terminal voltage transients.

5. Conclusions

A loop-shaping procedure has been employed to design a robust damping controller for a power system with SMES. The graphical loop-shaping technique selects the open loop transfer function and then determines the fixed parameter controller satisfying the robust stability and performance criteria. The robust design has been carried out considering a detailed 13th order model of the generator- SMES system. The controller designed was tested for a number of disturbance conditions including symmetrical three-phase faults. The robust design has been found to be very effective for damping control over a wide range of operating conditions of the power system. The operating conditions for which the controller provides good performance depends on the spectrum of perturbed plants selected in the design process. The graphical loop-shaping method utilized to determine the controller function is simple and is straightforward to implement. For implementation of this design in a multi-machine power system, decentralized robust controllers can be used for each area in the system.

References

[1] Peterson AH, Mohan N, Broom RW. Super-conducting energy storage inductor-converter units for power systems. IEEE Trans Power Apparatus Syst 1975;94:1337–49.
[2] Shelton ML, Winkelman PF. Bonneville power administration 1400 MW braking resistors. IEEE Trans Power Appl Syst 1975;94:602–11.
[3] Rogers JD, Schermer RI, Miller RL, Hauer JF. 30 MJ superconducting magnetic energy storage system for electric utility transmission stabilization. Proceedings IEEE 1983;71(9):1099–107.
[4] Tan YL, Wang Y. Augmentation of transient stability using a superconducting coil and adaptive nonlinear control. IEEE Trans Power Syst 1988;13(2):361–6.
[5] Wu Y, Lee Y. Application of super-conducting magnetic energy storage unit to improve the damping of synchronous generators. IEEE Trans Energy Convers 1991;6(4):573–8.
[6] Rahim AHMA, Mohammad AM. Improvement of synchronous generator damping through super-conducting magnetic energy storage systems. IEEE Trans Energy Convers 1994;9(4):736–42.
[7] Mitani Y, Uranka T, Tsuji K. Power system stabilization by superconducting magnetic energy storage with solid-state phase shifter. IEEE Trans Power Syst 1995;10:1614–9.

[8] Wu C, Wang C. Damping power oscillations by an active and reactive power modulation superconducting magnetic energy storage unit. Electric Power Syst Res 1992;24:65–72.
[9] Chen N, Carroll DP. Damping control of power systems with magnetic energy storage. Int J Energy Syst 1990;10(2):78–82.
[10] Rabbani MG. An adaptive fuzzy controlled superconducting magnetic energy storage unit for power system. Energy Convers Manage 1988; 39:931.
[11] Devotta JBX, Rabbani MG, Elangovan S. Application of superconducting magnetic energy storage unit for damping of subsynchronous oscillations in power systems. Energy Convers Manage 1999;40:23–37.
[12] Pal BC, Cornick AH, Jaimoukha IM, El-Zobaidi H. A linear matrix inequality approach to robust damping control design in power systems with super-conducting magnetic energy storage device. IEEE Trans Power Syst 2000;15(1):356–62.
[13] Doyle JC, Francis BA, Tannenbaum AR. Feedback control theory. New York: Macmillan Publing; 1992.
[14] Song YH, Johns AT. Flexible AC transmission systems (FACTS). IEE Power and Energy Series 30: Inspec/IEE, 1999.
[15] Acha E, Fuerte-Esquivel CR, Ambiriz-Perez H, Angeles-Camacho C. FACTS Modeling and simulations in power networks. New York: Wiley; 2004.
[16] Machowski J, Nelles D. Optimal control of superconducting magnetic energy storage unit. Elect Mach Power Syst 1992;20(6): 623–40.
[17] Machowski J, Nelles D. Optimal modulation controller for superconducting magnetic energy storage. Int J Elect Power Energy Syst 1994;16(5):291–300.
[18] Chao A, Athans M. Stability robustness to unstructured uncertainty for linear time invariant systems. In: Levine WS, editor. The control handbook. CRC Press and IEEE Press; 1996.
[19] Dahleh MA. l_1 robust control: theory, computation and design. In: Levine WS, editor. The control handbook. CRC Press and IEEE Press; 1996.